Near-Field Polarization Effects in Molecular-Motion-Induced Photochemical Imaging

Christophe Hubert,*,† Renaud Bachelot,*,† Jérôme Plain,† Sergeï Kostcheev,† Gilles Lerondel,† Mathieu Juan,† Pascal Royer,† Shengli Zou,‡ George C. Schatz,§ Gary P. Wiederrecht,|| and Stephen K. Gray||

Laboratoire de Nanotechnologie et d'Instrumentation Optique, Université de Technologie de Troyes, Institut Charles Delaunay, CNRS-FRE 2848, 12 rue Marie-Curie, 10000 Troyes, France, Department of Chemistry, University of Central Florida, Orlando, Florida 32816-2366, Department of Chemistry, Northwestern University, Evanston, Illinois 60208, Center for Nanoscale Materials and Chemical Sciences and Engineering Division, Argonne National Laboratory, Argonne, Illinois 60439

Received: October 2, 2007; In Final Form: December 14, 2007

We demonstrate near-field polarization-sensitive photochemical imaging of the optical near fields produced by metal nanostructures under a variety of illumination conditions. The method relies on the optically induced vectorial molecular mass transport of a light-sensitive polymer. The experimental and theoretical results clearly show that this method can map the three spatial components of the optical near field of complex metal nanostructures. The method was applied to map the electromagnetic near field of silver bowtie nanostructures. In particular, we find that longitudinally polarized plasmons are confined at the top of the metallic structures. Furthermore, the intricate optical near fields in the polymer lead to molecular trapping regions at intensity minima.

Introduction

There has been considerable recent interest in the physics and applications of surface plasmon polaritons (SPPs).[1,2] Recently, we reported on the subdiffraction imaging of the optical near field in metal nanostructures based on a photochemical technique.[3] This approach relies on the photoinduced mass transport of azobenzene molecule-containing polymers coated onto the nanostructures. Migration of the azobenzene molecules, triggered by confined near fields, leads to topographic modifications at the polymer film surface that are then measured by atomic force microscopy (AFM). The spatial features of the induced topography give insight into the near-field spatial profile produced by the metal nanostructures and can highlight different physical phenomena. These include, for example, localized surface plasmons and lightning rod effects. As with near-field optical scanning probe methods,[4−6] this photochemical imaging approach can provide spatial resolution better than the diffraction limit of conventional microscopes. Optical scanning probe experiments, however, are often time consuming and the probe itself can modify the optical near field being measured. Photochemical imaging is an alternative or complementary approach that is relatively fast and does not involve any direct interactions of the probe with the near fields. It can also be used to study fundamental issues regarding molecular transport in intense and confined optical fields.

The optical response of azodye molecules embedded in polymers has been shown to be strongly sensitive to the polarization state of the electromagnetic field experienced by the molecules.[7−11] In our work here it is the enhanced optical near fields produced through the interaction of the incident field with the metal nanoparticles that dominate the polymer response. We define transverse and longitudinal polarization directions in terms of the incident light propagation direction, with longitudinal polarization along the incident light propagation direction. Previous studies show that the polymer moves laterally away from the optical field maxima for transverse polarization,[9−11] while longitudinal field components tend to lift the matter vertically as a consequence of the free space requirement of the molecules.[7,8] These two modes of matter migration have been observed simultaneously for fields involved in delocalized surface plasmon interference,[12] scattering by a nanometer-sized metal tip,[13] and strong localization of high-order beams by a high-numerical-aperture objective.[7]

The different molecular transport responses to polarized fields present an interesting opportunity to use photochemically responsive materials to extract individual field polarization components from the total field. Here we report, for the first time to our knowledge, a photochemical vectorial imaging of the three spatial components of the optical electromagnetic near field of complex metal nanostructures. In particular, the spatial orientation of the longitudinally polarized electromagnetic near field from a silver bowtie nanoantenna is observed and shown to strongly depend on the near-field spatial profiles that are altered with incident light polarization. The results reveal longitudinal plasmon fields confined at the tops of the metallic structures that are believed to function as a plasmonic cavity, with the reflected plasmon producing self-interference and a standing wave pattern.[14] The results are only detectable due to the ability of the polymer to respond specifically to the longitudinal fields while other field polarizations are present. These structures are also shown to produce spatial near-field

* To whom correspondence should be addressed. C.H.: present address Laboratoire Hubert Curien, UMR-CNRS 5516, Université Jean-Monnet, 18 rue du professeur benoît Lauras, 42000 St-Etienne; phone, +33 (0) 4 77 91 58 23; fax, +33 (0) 4 77 91 57 81; e-mail, Christophe.hubert@univ-st-etienne.fr. R.B.: e-mail: renaud.bachelot@utt.fr.
† Université de Technologie de Troyes.
‡ University of Central Florida.
§ Northwestern University.
|| Argonne National Laboratory.

10.1021/jp7096263 CCC: $40.75
Published on Web 02/26/2008

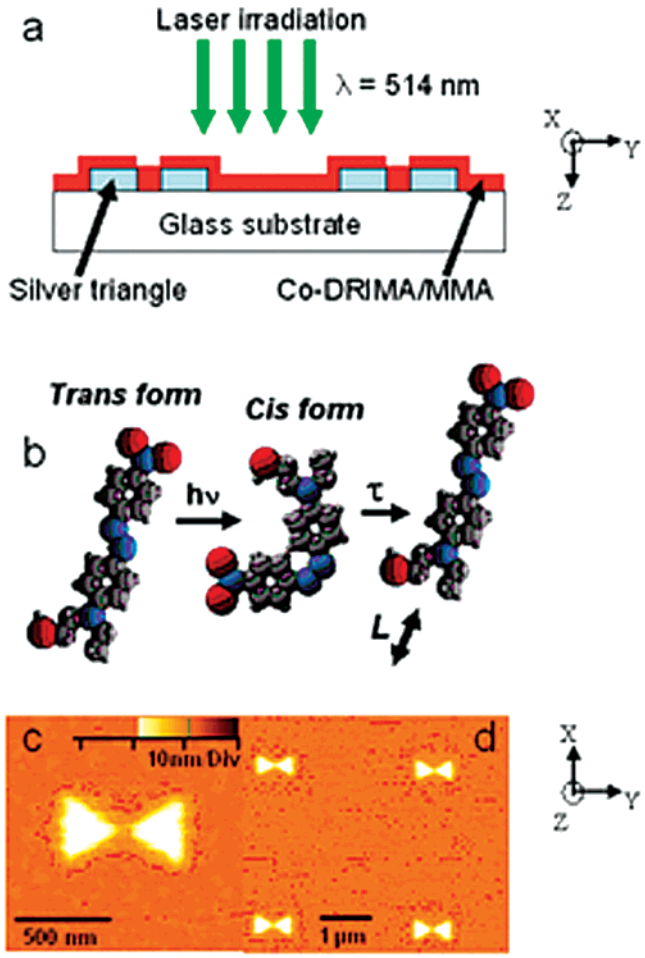

Figure 1. Schematic view of the approach. (a) The metallic nanostructures are coated with DR1MA/MMA copolymer and then irradiated at normal incidence by the 514 nm laser line of an argon-ion laser. (b) The conformation modification between the trans and cis form of the DR1 azodye molecule as well as its translational movement after relaxation is indicated. (c and d) Atomic force microscopy (AFM) images of the surface sample after spin coating of the copolymer and before irradiation.

profiles with multiple "hot spots" that serve to drive and trap molecular species at specified locations.

Methods

The experimental approach used in this study has been described in previous work[1] and is briefly summarized below (Figure 1a). Metal nanostructures were fabricated by electron-beam lithography through the lift-off method. The azodye molecule-containing polymer consists of the azo-dye molecule Dispersed Red 1 [4-(*N*-(2-hydroxyethyl)-*N*-ethyl)amino-4′-nitroazobenzene] (DR1) grafted as a side chain to PMMA in a 30% molar ratio (DR1MA/MMA). DR1MA/MMA is then dissolved in 1,1,2-trichloroethane and spin coated onto the nanostructures. AFM measurements show that after spin coating the metal structure, the DR1MA/MMA film is about 100 nm thick, with 50 nm above the nanoparticles. This film thickness is within the evanescent near-field decay length of 50−100 nm for these types of silver nanoparticle structures.[4,6] This thickness reliably produced homogeneous films, although thinner films should produce improved spatial resolution. No drying is performed after spin coating in order to simulate a low glass-transition polymer, which is known to improve azo-dye transport.[15] Irradiation of the sample is performed with normal incidence relative to the sample using the 514 nm line of an argon-ion laser. The samples were irradiated for 20 min and with an intensity of 100 mW/cm^2. Following irradiation of the polymer within the absorption band of DR1, the molecules will undergo trans−cis photoisomerization. Note that with polarized light those molecules oriented with their transition moment parallel to the illumination field will be preferentially excited. This is followed by relaxation of DR1 molecules back to their trans form after an average translation L parallel to their molecular axis (Figure 1b). Surface effects are thus governed by photon-assisted molecular diffusion, with the azo-dye molecules playing the role of molecular motors that push or pull the polymeric host along the polarization of the incident field. This leads to a photoinduced mass transport that produces surface topography after irradiation that is characterized using an AFM. In such an experiment, each molecule acts as a nanoprobe of the optical near field of the nanostructures. Atomic force microscopy images of the sample surface after spin coating and before irradiation are shown in Figure 1c,d. The color scale on the AFM images is such that white is high and black is low.

The sample consists of 5 μm periodic arrays of silver bowtie nanoparticles with a height of 50 nm and bowtie gap width of 80 nm. The triangles in the bowties are 400 nm in length. Such structures are generally expected to act as efficient optical antennas.[16−19] However, due to our lithographic fabrication process, the bowtie nanoparticles here have such radii of curvature that a pronounced antenna effect does not appear.

Theoretical modeling is used to support the experimental observations. We used the discrete dipole approximation (DDA)[20−22] to model the electric field distribution around a bowtie composed of two silver triangles. Schatz and co-workers have shown that DDA can accurately describe plasmon excitations in a variety of metallic nanostructures.[21,22] In a DDA calculation, the metal nanoparticles are described by an array of point dipoles and one solves a set of complex, linear equations to obtain the polarizations that result from the dipoles in response to an incident field. The grid resolution in the DDA method is chosen to be 5 nm, and the working wavelength is 514 nm. The length of each particle is 400 nm, and the height is 50 nm, which are the same as in the experiments. The polarization is selected to be parallel to either the Y or X axis shown in Figure 1. Y is the major axis of the dimer, X is the minor axis, and Z is the light propagation axis. Z also corresponds to the direction of the longitudinal fields that are highlighted in this paper. The bowtie gap is set to be 80 nm. The particles are embedded in the DR1MA/MMA copolymer with an index of refraction estimated to be $n_{poly} = 1.72$ or dielectric constant $\epsilon_{poly} = n_{poly}^2 = 2.96$, based on prior DR1MA/MMA studies.[3] The dielectric constant for Ag at 514 nm is taken to be $\epsilon_{Ag} \approx -9.26 + 0.79i$.[23] The planes of the subsequent image plots are chosen to be perpendicular to the incident wave. The total electric field intensity ($|E_{tot}|^2$) and its component contributions ($|E_X|^2$,$|E_Y|^2$,$|E_Z|^2$) are calculated on a plane 5 nm above the particle surfaces. This is a relevant plane where the field is expected to be mainly evanescent and spatially confined. As outlined above, the film thickness was determined by the need for a homogeneous film, and thinner films would produce even higher spatial resolution.

Results and Discussion

Figure 2a−c shows AFM images of the sample surface after irradiation for an incident polarization of the laser beam oriented along X, i.e., perpendicular to the major axis of the bowtie. The theoretical near-field intensities that result when a silver bowtie

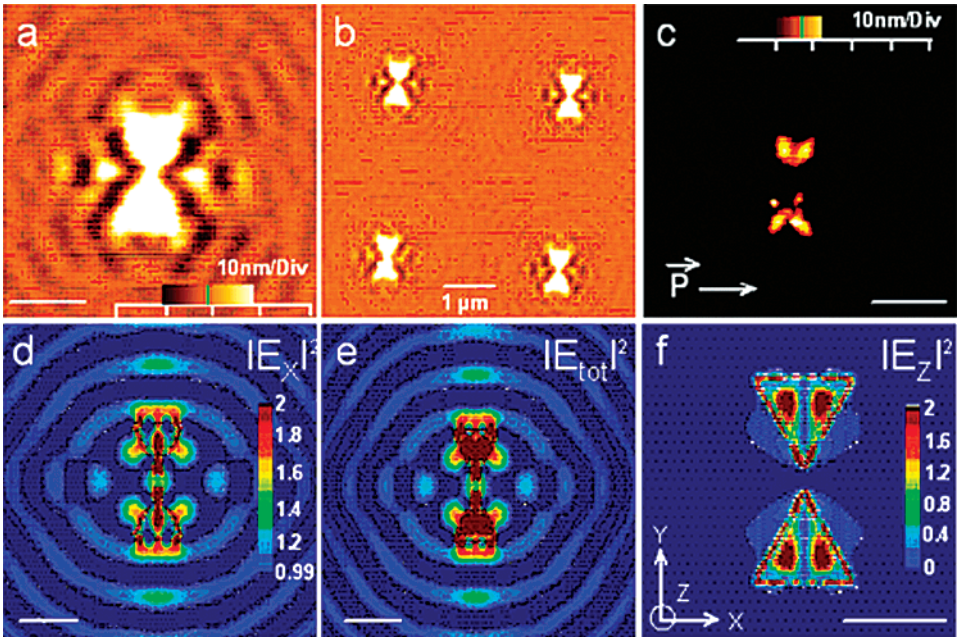

Figure 2. AFM images of the sample surface after irradiation (a−c). (c) Obtained by adjusting the contrast level of image a. The incident light polarization, represented in c, was parallel to the *X* axis, i.e., perpendicular to the bowtie major axis. Calculated $|E|^2$ contour plots for *X*-polarized incident light in a plane 5 nm above the particle surface are given (d−f). (d) $|E_X|^2$, (e) $|E_{tot}|^2$, (f) $|E_Z|^2$. The color scale in d−f is such that brown is high and blue is low. The scale bar represents 500 nm unless otherwise noted.

is exposed to $\lambda_0 = 514$ nm light, calculated with the DDA method, are given in Figure 2d−f. Large topographic modifications are observed in Figure 2a and b. In Figure 2a, topographic minima (depth and width of about 10 and 170 nm) can be observed along the edges of the triangles as well as two principal topographic maxima (height of about 10 nm) localized symmetrically with regard to the nanostructures and along the *X* direction. These results can be compared to the theoretical electric field intensity associated with just the lateral *X* component, $|E_X|^2$ (Figure 2d). Topographic minima are observed at the same position as the field maxima localized on the edges of the nanostructures, which is consistent with the fact that in the case of incident polarization oriented in the plane of the sample the matter escapes from high-intensity regions to low-intensity regions.[9−11] Molecular migration stops, i.e., accumulation of copolymer and thus topographic maxima, when the molecules are no longer excited, i.e., where there are field minima positions. This explains the two topographic maxima which originate from photoinduced mass transport from regions of electric field maxima toward regions of electric field minima. We note that intensity variations within high-field regions can additionally influence polymer migration. For example, for the high-field region in the gap between the nanoparticle triangles, the transverse $|E_X|^2$ optical near-field intensity (Figure 2d) shows two narrow high-field lines that appear to contain polymer material, minimizing the appearance of a dip between the triangles.

An interference fringe system can also be observed in the topographic image (Figure 2a). These fringes are only visible along the *X* direction and only extremely weakly in the *Y* direction, in contrast to the calculation where fringes can be observed in both directions. This originates from the fact that in the case of electric field components in the plane of the sample the maximum efficiency of molecular migration occurs when the electric field has a nonzero component along the light intensity gradient.[11] This condition is fulfilled in the experimental results presented in Figure 2 only when the incident electric field polarization is oriented along the *X* direction, leading to formation of fringes in the topographical images.

Calculations indicate that almost no lateral $X \rightarrow Y$ depolarization occurs (not shown here) but that a significant $X \rightarrow Z$ depolarization can be observed as shown in Figure 2f. This is also in good agreement with experimental observations reported here. This effect of lateral → longitudinal near-field depolarization is well known and was recently reported in the case of metal tip.[13] Experimentally, it can be highlighted when adjusting the contrast level of Figure 2a where a numerical threshold process gives insight into high-topography zones. The result is shown in Figure 2c and shows that the copolymer accumulates on top of the two silver triangles. This can be directly compared to the calculated longitudinal intensity component $|E_Z|^2$ presented in Figure 2f. The results show that the longitudinal field maxima are localized at the same position as the topographic maxima observed on the AFM image in Figure 2c.

Given the relatively large size of the triangle faces in the bowties, the primary localized surface plasmon resonance is expected to occur at a significantly longer wavelength than our incident wavelength of $\lambda_0 = 514$ nm. In fact, DDA calculations of the extinction spectrum (not shown) give a large, broad resonance in the 1500−2500 nm regime. For flat metal surfaces, of course, propagating SPPs can exist at any wavelength for which the metallic dielectric constant has a negative real part. One interpretation of the lobed feature in Figure 2c (or Figure 2f) is that it arises from a standing wave produced through superposition of counter-propagating SPPs on the metal surface, $\exp(-ik_{SPP}X) + \exp(ik_{SPP}X) \propto \cos(k_{SPP}X)$. This would give an intensity proportional to $\cos^2(k_{SPP}X) = \cos^2(2\pi X/\lambda_{SPP})$ with adjacent maxima separated by $\lambda_{SPP}/2$. Note that the counter-propagating wave could be due to self-reflection of an SPP off the particle edges. Thus, the particles may be acting as a kind of plasmonic cavity.[14] The SPP wavelength consistent with the Ag/polymer interface is estimated to be[24] λ_{SPP} (Ag/polymer) = λ_0 Re$[(\epsilon_{Ag} + \epsilon_{poly})/(\epsilon_{Ag}\epsilon_{poly})]^{1/2} \approx 247$ nm at $\lambda_0 = 514$ nm. Note that owing to the finite thickness of the polymer over the

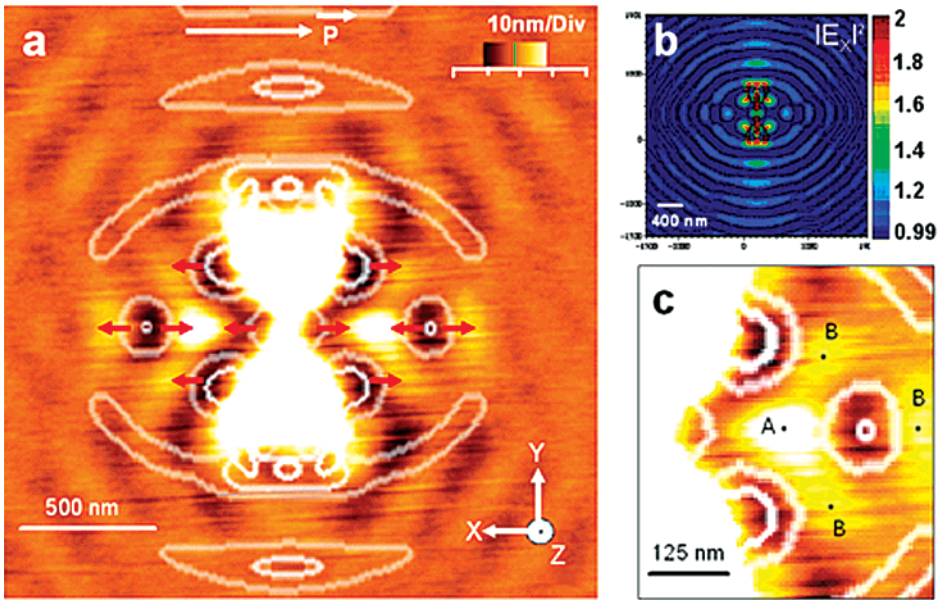

Figure 3. Evidence for molecular optical trapping of azobenzene molecules by transverse fields. (a) Photoinduced topography for the case of the *X*-polarized incident light superposed with the calculated $|E_X|^2$ intensity. (b) The $|E_X|^2$ spatial profile is shown as a reminder. (c) Locations of molecular trapping by the optical fields produced by the nanostructure. Point A is the result of two high-field regions that push molecular material into this region. Points labeled B are produced by mass transport from one high-field region. The scale bar represents 500 nm unless otherwise noted.

metal, it is likely that the effective index is smaller than that for the bulk polymer, so that the actual SPP wavelength would be correspondingly somewhere between λ_{SPP}(Ag/polymer) = 247 and λ_{SPP}(Ag/air) = 486 nm.[25] Both the experimental (Figure 2c) and theoretical (Figure 2f) images have maxima separated by ~160−180 nm, implying an effective SPP wavelength of ~320−360 nm, which is consistent with this simple analysis.

Figure 2 also shows that the propagation axis associated with the counter-propagating SPP waves is along the polarization direction of the incident field. This observation unambiguously demonstrates that azo-dye molecules are very sensitive to the longitudinal component of the light electric field, leading to high topography contrast. It should be pointed out that this longitudinal field is purely perpendicular to the structure's top surface. It is thus discontinuous at the interface and strongly influenced by surface charge density. Our method allows a direct visualization of the surface charge density at the top of the surface. Figure 2 thus shows that when the incident electric field has transverse components, mass transport occurs from high- to low-intensity regions in the plane of the sample along the incident light polarization direction, whereas when longitudinal components exist, azo-dye molecules preferentially migrate upward, toward the free surface of the polymer film.

It should be stressed that the transverse sensitivity allows for nanoscale optical trapping of azobenzene molecules. This effect is highlighted in Figure 3, where the theoretical $|E_X|^2$ map is superposed with the topography deduced from our AFM measurements. In Figure 3a, red arrows emphasize the migration direction. In the magnified portion in Figure 3c, point A represents molecular accumulation due to optical trapping by two surrounding electromagnetic hot spots while points labeled B are produced from a single nearby hot spot. The image in Figure 3a shows that the topography change scales with the number of electromagnetic hot spots present in the vicinity. This example nicely illustrates the possibility of molecular optical trapping by complex metal nanostructures.

The AFM images presented in Figure 4a−c show the sample surface after irradiation with an incident light polarization oriented parallel to the bowtie major axis, i.e., along the *Y* axis. The topographic modifications observed at the polymer film surface in Figure 4a are in good agreement with the theoretical calculation of $|E_Y|^2$ shown in Figure 4d. The two electric field maxima located on the edges of the triangles in the *X* direction lead to topographic minima observed on the AFM image as well as to the two topographic maxima which originate from a molecular migration phenomenon photoinduced from high electromagnetic field intensity toward a low-intensity region. In the case of the incident *Y* polarization, *Y* and *Z* fields are primarily produced, leading to possible molecular migration along these directions. Again, both computational and experimental results indicate that there is little depolarization in the *X*−*Y* plane. Since the incident laser beam polarization is oriented in the *Y* direction, as well as the light intensity gradient, the migration of the azo-dye molecules in the plane of the sample is preferentially driven in the *Y* direction. This leads to the topographic minima observed on the top and bottom edges of the nanostructures which are photoinduced by the intensity maxima observed at the same position on the numerical calculation. We note that while Figures 2a and 4a have similar features regarding the high-topography lobes on either side of the gap along the *X* axis, the lobes have different center-to-center distances. This specifically is due to the fact that the two topography lobes in Figure 4 originate from the four *Y* polarized bright spots close to the triangle corner, leading to two topographical bright spots seen symmetrically from the center of the bowtie. On the other hand, the two bright spots seen in Figure 2 originate from a trapping by different *X*-polarized bright spots (please see overlay in Figure 3). This difference in origin is confirmed by the fact that the distance between the two bright spots in Figure 4 is smaller than that observed in Figure 2. An interference fringe system is again observed on the topographic image in Figure 4a. In this case, the fringes are only visible along the *Y* direction and can again be explained by the fact that the involved electric field polarization is oriented in the plane of the sample, parallel to the light intensity gradient, which is not the case for the *X* direction.

Topographic maxima are also observed on the top of the triangles in Figure 4c, their shape being different from the ones

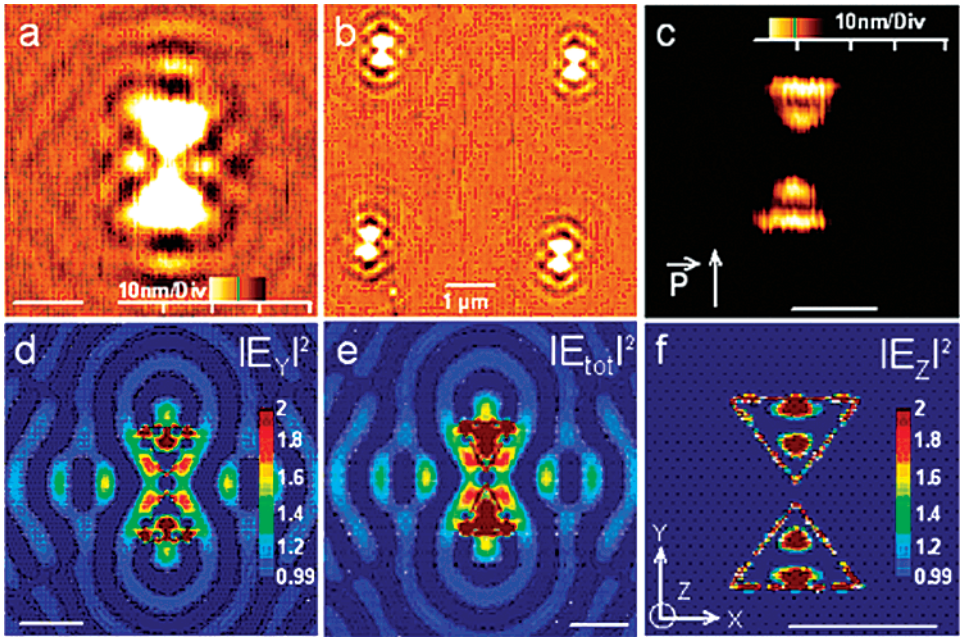

Figure 4. AFM images of the sample surface after irradiation (a−c). (c) Obtained by adjusting the contrast level on image a. The incident polarization, represented in c, was parallel to the bowtie major *Y* axis. Intensity $|E|^2$ calculated contour plots for *Y*-polarized incident light in a plane 5 nm above the particle surface: (d) $|E_Y|^2$, (e) total intensity, (f) $|E_Z|^2$. The color scale in d−f is such that brown is high and blue is low. The scale bar represents 500 nm unless otherwise noted.

observed in Figure 2c. These maxima must be compared to the calculated longitudinal field intensity $|E_Z|^2$ presented in Figure 4f and definitively confirm the fact that azo-dye molecules are also sensitive to the longitudinal vectorial component of the incident electric field: longitudinal field components tend to lift the matter vertically as a consequence of free space requirement from the molecules. Importantly, the lobed spatial features are very similar to the features seen for *X*-polarized excitation in Figure 2c and f but with an orthogonal fringe pattern. These features are again strongly supportive of a SPP standing wave along the polarization direction, with the edges of the nanoparticle possibly serving as a cavity to reflect the plasmon. A standing wave through self-interference of the plasmon with the reflected plasmon is again created, with interference fringes orthogonal to those for *X*-polarized illumination. As with our analysis of the *X* polarization case (Figure 2), we can associate the effective SPP wavelength for this longitudinal polarization case with twice the distance between maxima. The experimental (Figure 4c) and theoretical (Figure 4f) effective SPP wavelengths, roughly equal to 180 nm, are in good accord and consistent with our analysis of Figure 2.

Conclusions

The results presented in this work unambiguously demonstrate the ability of azo-dye molecules embedded in a polymer to function as a nanoprobe for nanoscale imaging of the three different components of the near-field electromagnetic wave. While the polymer moves laterally away from the field maxima for transverse polarizations, longitudinal field components tend to lift the matter vertically as a consequence of the free space requirement from the molecules. This feature permits the observation of standing waves in the plasmonic nanostructures by selecting longitudinally polarized fields out of the total field. Our photochemical imaging technique with these materials open new routes toward a better understanding of the near-field light intensity distribution around complex metallic nanostructures. It is also a means of studying other physical phenomena, such as molecular trapping and transport induced by near fields.

Acknowledgment. The work at the Université de Technologie de Troyes was partly supported by the Region Champagne Ardenne under the contract "Projet émergence : Photoélaboration en champ proche de nouvelles particules hybrides pour la nanophotonique" and partly supported by the National Research Agency under the contract "ANR-PHOTOHYBRID". The work at Argonne was supported by the U.S. Department of Energy, Office of Science, Office of Basic Energy Sciences, under contract no. DE-AC02-06CH11357. G.C.S. and S.Z. were supported by the U.S. Department of Energy under grant no. DEFG02-03-ER15487 and the Northwestern Materials Research Center, sponsored by the National Science Foundation (DMR-0520513). S.Z. also thanks the University of Central Florida for support from a start-up fund. The authors would like to acknowledge Pierre-Michel Adam for fruitful discussions.

References and Notes

(1) Zayats, A. V.; Smolyaninov, I. *J. Opt. A: Pure Appl. Opt.* **2003**, *5*, 16.
(2) Wurtz, G. A.; Hranisavljevic, J.; Wiederrecht, G. P. *Nano Lett.* **2003**, *3*, 1511.
(3) Hubert, C.; Rumyantseva, A.; Lerondel, G.; Grand, J.; Kostcheev, S.; Billot, L.; Vial, A.; Bachelot, R.; Royer, P.; Chang, S. H.; Gray, S. K.; Wiederrecht, G. P.; Schatz, G. C. *Nano Lett.* **2005**, *4*, 615.
(4) Courjon, D. *Near-field Microscopy and Near-Field Optics*; Imperial College Press: Singapore, 2003.
(5) Novotny, L.; Stranick, S. J. *Annu. Rev. Phys. Chem.* **2006**, *57*, 303.
(6) Wiederrecht, G. P. *Eur. Phys. J. Appl. Phys.* **2004**, *28*, 3.
(7) Gilbert, Y.; Bachelot, R.; Royer, P.; Bouhelier, A.; Wiederrecht, G. P.; Novotny, L. *Opt. Lett.* **2006**, *31*, 613.
(8) Grosjean, T.; Courjon, D. *Opt. Exp.* **2006**, *14*, 2203.
(9) Cojocariu, C.; Rochon, P. *Pure Appl. Chem.* **2004**, *76*, 1479.
(10) Lefin, P.; Fiorini, C.; Nunzi, J. M. *Pure Appl. Opt.* **1998**, *7*, 71.
(11) Ishitobi, H.; Tanabe, M.; Sekkat, Z.; Kawata, S. *Opt. Express* **2006**, *15*, 652.

(12) Derouard, M.; Hazart, J.; Lérondel, G.; Bachelot, R.; Adam, P. M.; Royer, P. *Opt. Express* **2007**, *15*, 4246.
(13) Gilbert, Y.; Bachelot, R.; Vial, A.; Lerondel, G.; Royer, P.; Bouhelier, A.; Wiederrecht, G. P. *Opt. Express* **2005**, *13*, 3619.
(14) Egusa, S.; Liau, Y. H.; Scherer, N. F. *Appl. Phys. Lett.* **2004**, *84*, 1257.
(15) Slark, A. T.; Hadgett, P. M. *Polymer* **1999**, *40*, 4001.
(16) Grober, R. D.; Schoelkopf, R. J.; Prober, D. E. *Appl. Phys. Lett*. **1997**, *70*, 1354.
(17) Farahani, J. N.; Eisler, H. J.; Pohl, D. W.; Pavius, M.; Flückiger, P.; Gasser, P.; Hecht, B. *Nanotechnology* **2007**, *18*, 125506.
(18) Schuck, P. J.; Fromm, D. P.; Sundaramurthy, A.; Kino, G. S.; Moerner, W. E. *Phys. Rev. Lett.* **2005**, *94*, 017402.
(19) Sundaramurthy, A.; Schuck, P. J.; Conley, N. R.; Fromm, D. P.; Kino, G. S.; Moerner, W. E. *Nano Lett.* **2006**, *6*, 355.
(20) Draine, B. T.; Flatau, P. J. *J. Opt. Soc. Am. A* **1994**, *11*, 1491.
(21) Yang, W. H.; Schatz, G. C.; Van Duyne, R. P. *J. Chem. Phys.* **1995**, *103*, 869.
(22) Kelly, K. L; Coronado, E.; Zhao, L. L.; Schatz, G. C. *J. Phys. Chem. B* **2003**, *107*, 668.
(23) Palik, E. D. *Handbook of Optical Constants of Solids*; Academic Press: New York, 1985.
(24) Raether, H. *Surface Plasmons on Smooth and Rough Surfaces and on Gratings*; Springer-Verlag: New York, 1988.
(25) Ibn El Ahrach, H.; Bachelot, R.; Vial, A.; Lerondel, G.; Plain, J.; Royer, P.; Soppera O. *Phys. Rev. Lett.* **2007**, *98*, 107402.